A node activation based routing scheme in micro/nanobots networks

Yen, Hong-Hsu; Wang, Xinheng; Wang, Dong; Liaw, Horng-Twu

Published in:
IEEE Access

DOI:
10.1109/ACCESS.2019.2945070

Published: 02/10/2019

Document Version
Publisher's PDF, also known as Version of record

IEEE Access
Multidisciplinary | Rapid Review | Open Access Journal

Received August 12, 2019, accepted September 10, 2019, date of publication October 2, 2019, date of current version October 16, 2019.

Digital Object Identifier 10.1109/ACCESS.2019.2945070

A Node Activation-Based Routing Scheme in Micro/Nanobots Networks

HONG-HSU YEN[1], (Member, IEEE), XINHENG WANG[2], (Senior Member, IEEE), DONG WANG[3], (Student Member, IEEE), AND HORNG-TWU LIAW[1], (Student Member, IEEE)

[1]Department of Information Management, Shih Hsin University, Taipei 116, Taiwan
[2]Department of Electrical and Electronic Engineering, Xi'an Jiaotong-Liverpool University, Suzhou 215123, China
[3]School of Computing, Engineering and Physical Sciences, University of the West of Scotland, Glasgow G72 0LH, U.K.

Corresponding author: Hong-Hsu Yen (honghsuyen@gmail.com)

This work was supported in part by the Taiwan Ministry of Science and Technology under Grant MOST 107-2410-H-128-015.

ABSTRACT The rapid advancements of Micro/NanoBOTs (MNBOTs) introduce a new research opportunity in routing multiple MNBOTs to perform practical biomedical applications. In this paper, leveraging on existing group communication and motion control schemes for MNBOTs, we propose an Activation Based Molecular Routing (ABMR) scheme in MNBOT networks to coordinate the movement of MNBOTs to activate all the nodes on the routing path to the sink node in bio-sensing applications. An optimization-based algorithm, Lagrangian Algorithm (LGA), is proposed to identify cost efficient ABMR solutions. In the computation experiments, we adopt the MNBOT's parameters from a newly developed biocompatible microcapsule to consider the interplay between the MNBOT guiding force from magnetic field and the MNBOT movement deviation from Brownian motion. It shows that as compared to the conventional diffusion based MNBOT routing scheme, MNBOT routing with magnetic guidance scheme can help to reach the destinations with small receiving volume in shorter propagation time, which is important in high precision bio-medical applications. In addition, LGA outperforms the other heuristics in terms of MNBOT travelled distance under different traffic demands and activation thresholds. LGA also identifies the MNBOT routing decisions with acceptable sink node activation time by minimizing the MNBOT propagation delay as the objective function. This enables ABMR scheme to be applicable to time sensitive biosensing applications.

INDEX TERMS Micro/nanobots, molecular communication, molecular routing, node activation property, biological communication process.

I. INTRODUCTION

With the advance of nanotechnologies, the size of micrometers to nanometers Micro/NanoBOTs (MNBOTs) are now available [1]. Even though the MNBOT research is still in its early stage, the benefits from down to the cellular level diagnosis and treatment shed light on new biomedical procedure to conventionally inaccessible parts of the animals or plants. Numerous research efforts have been done to enable MNBOTs on more practical biomedical applications, such as therapeutic payloads delivery to target disease sites [2], high precision surgery at cellular level [3], bio-sensing capability in recognition of specific Alzheimer biomarker protein [4], and bio-detoxification in biological fluids [5].

The associate editor coordinating the review of this manuscript and approving it for publication was A. Taufiq Asyhari.

MNBOT guiding mechanism is important to enable MNBOT in biomedical applications. Individual navigation and speed control schemes of MNBOTs have been explored in existing research results. However, the group communication and synchronized coordination between a swarm of MNBOTs (or MNBOT networks) to perform more practical tasks in biomedical application is still a challenging issue [1].

In this paper, we address the MNBOT routing scheme that captures the node activation property in existing biological communication processes. In existing biological processes, cells receiving enough signaling molecules will be activated and released, signaling molecules to activate the other cells to propagate the signal. By carrying the signaling molecules in MNBOT, MNBOT transportation with guided orientation can react to the event faster than molecular diffusion scheme in existing biological processes. In Figure 1, we illustrate a biosensing example to show the differences between

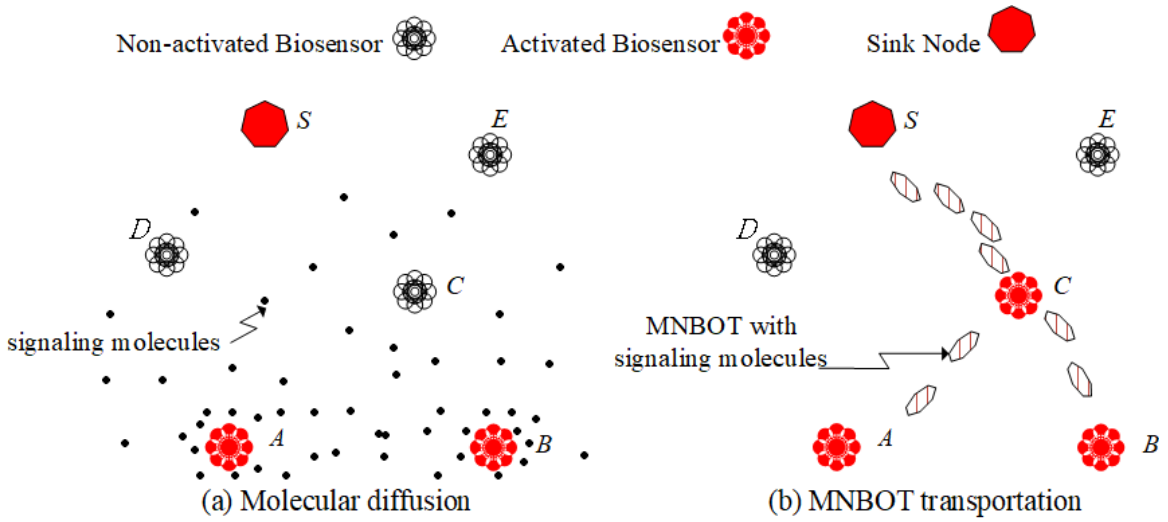

FIGURE 1. Molecular diffusion and MNBOT transportation in biosensing applications.

molecular diffusion and MNBOT transportation in activation-based signal propagation.

In Figure 1, the biosensors that sense the event (i.e., node *A* and *B*) release the signaling molecules to activate the relay nodes on the routing path and eventually activate the sink node. In Figure 1(a), the signaling molecules release by node A and node *B* will follow the Brownian motion incurred molecular diffusion process that flow randomly in the biological fluids. In Figure 1(b), MNBOTs carrying the signaling molecules as the payload will move on the routing path to activate the relay node *C* and eventually activate the sink node *S*. Apparently, MNBOT transportation scheme require much lesser signaling molecules and lesser time to activate the sink node than the molecular diffusion scheme. However, the trajectory path of MNBOT still suffers the interference from Brownian motion in the high viscous biological fluids. Devising a MNBOT routing scheme with considering the activation constraint and Brownian motion interference will be an interesting problem. In this paper, we devise an efficient activation-based routing scheme in MNBOT networks that addresses the molecular collision interference.

In Section II, we will show the existing researches that enable MNBOTs networks to be a viable solution in biomedical applications. In Section III, we will devise a EMAR model to capture the node activation property and Brownian motion interference in MNBOT routing. In Section IV, the optimization-based approach, the complete algorithm Lagrangian Algorithm (LGA), is proposed to solve this MNBOT routing problem. In Section V, the computational experiments will be performed to evaluate the solution quality of the LGA algorithm. In Section VI, we will conclude this paper.

II. RELATED WORKS

A. RESEARCH ON BIOCOMPATIBLE MNBOTS

Bio-compatibility is one of the major concerns when implanting MNBOTs into the animal's body. A lot of research efforts in chemistry and material science have been made in building bio-compatible MNBOTs. The basic idea of these works is not only to make the MNBOTs non-toxic, but also biodegradable after their mission is accomplished [6]. In addition to the material composition of the MNBOTs, the bio-compatible fuels and the byproducts after chemical reactions to propel the MNBOTs are also studied in numerous research efforts. MNBOT can either carry the fuel [12] or draw in fuels from the surrounding biological fluids [7] to propel the MNBOT. The second approach raises more attention in recent years where the MNBOT is fabricated with catalytic materials (e.g., Zn, Mg) in its hollow propulsion chamber. MNBOT draws in fuels (e.g., acid, water) from its surrounding environment to react with the catalyst in the hollow chamber to produce hydrogen bubbles to propel the MNBOT [7].

Besides the MNBOT hardware, the communication scheme between these MNBOTs should also be bio-compatible. One of the bio-compatible communication schemes is molecular communication [8], which is leveraged on existing biological cellular communication processes. Besides bio-compatibility, molecular communication requires very little energy to generate and propagate [9]. Basically, there are two molecular communication schemes in MNBOTs. In the first scheme, MNBOT releases the signaling molecules and the molecules move either by diffusion or fluid flow. Molecular diffusion is observed in existing biological processes and some existing works have developed in-depth theoretical results for the end-to-end molecular diffusion model [10] and the modulation scheme in considering the oscillating and propagating patterns in biological cells [11]. However, molecular diffusion incurred by the Brownian motion suffers from low propagation speed and turbulent flow in the biological fluid. In the second scheme, self-propelled MNBOT is introduced to transport and release the payloads (i.e., signaling molecules or drug particles) to the target place. The velocity of the self-propelled MNBOT can be extremely fast, up to hundreds of MNBOT's body length

per second [7]. This makes self-propelled MNBOT a more promising scheme in molecular communication processes, which is adopted in this paper. We will show in the latter, computational experiments that molecular diffusion-based scheme is not applicable to the high precision bio-medical applications.

B. RESEARCH ON MOTION CONTROL

To be applicable in biomedical applications, motion control (speed control and navigation) mechanisms are proposed for self-propelled MNBOTs to overcome the Brownian motion and high viscous force in the body fluid. Studies show that by using the external stimuli from Ultraviolet (UV) light [14] and ultrasound fields [15], the speed to generate the bubbles can be controlled to trigger the activation and deactivation of the MNBOT's motion. One of the most commonly used technique in MNBOT navigation is to integrate the ferromagnetic layer (e.g, Fe, Zn) into the tubular structure of MNBOT and using external magnetic field to navigate the MNBOT [13]. The magnetic field can be generated by magnets [13] or magnetic coils [31].

Group MNBOTs navigation scheme is first proposed in [31] to guide the ferromagnetic MNBOTs via the magnetic field generated by the magnetic coils deployed in the networks. By controlling the input currents to the micro-coils on the nodes in the bio-sensing networks, the nodes generate the attractive magnetic potentials (negative input current) and repulsive magnetic potentials (positive input current) to the positive charged ferromagnetic MNBOTs. Then, magnetic potential field navigation is possible to guide and control the trajectory path of the ferromagnetic MNBOTs along the desired path.

C. RESEARCH ON MNBOT HARDWARE CAPABILITIES

To realize group communication and coordination between the MNBOTs, three major hardware capabilities (i.e., *computing*, *storage* and *communication*) of MNBOTs are required. In [16], the first molecular computer chip with 160 Kbits was built based on a molecular machine, rotaxane. The inventors of the rotaxane, Stoddart et al., are awarded 2016 Nobel prize in Chemistry [17]. Rotaxane is an electron-poor ring-shaped molecule that is attached to an axle with electron-rich structures in two places [18]. By heating rotaxane, the ring jumps forward and backward between the electron-rich areas of the axle, which acts like a shuttle with on-off capability [19]. Rotaxane molecular machine realizes the computing and storage capabilities in MNBOTs.

In [33], Jensen*et al.* developed new Carbon Nano Tubes (CNT) that can transmit/receive wireless signals. In [34], Jornet *et al.* propose a CNT based modulation and channel access scheme, called Time Spread On-Off Keying (TS-OOK), in the Terahertz band. The basic idea of the TS-OOK is to generate short pulses (one hundred femtoseconds long) in the Terahertz band and the achievable data rate can achieve Gbps to Tbps. By equipping a CNT radio, high data rate wireless communications are achievable in MNBOTs. With the capabilities of computing, storage and communication in micro/nano-scale machines, it is now possible to coordinate and route multiple MNBOTs to perform more sophisticated bio-medical tasks.

D. RESEARCH ON NODE ACTIVATION PROPERTY

In this paper, we address the MNBOT routing scheme that captures the node activation property in existing biological communication processes. In existing biological processes, cells receiving enough molecules will be activated and released signaling molecules to activate the other cells to propagate the signal. In [20], they show that pain propagation comes from the activated nociceptors releasing the molecules to propagate the pain messages. After intense stimulation or persistent injury, activated nociceptors residing within injured area will release a variety of neurontransmitters and molecules to facilitate the transmission of pain messages to the brain. In [21], they conduct the in-vivo experiment to identify the pain activation threshold to activate the C fiber in human and rat. Besides pain propagation, molecular activation property is also observed in long range neural signal propagation. In [22], it is shown that protein kinase cascade can convey long distance phosphorylation waves. The ppMAPK (bisphos- phorylated mitogen-activated protein kinase) wave is supported by the feedback activation of MAP2K (MAPK, MAPK kinase). A two-site MAPK (de)phosphorylation bi-stable cycle generates a constant amplitude and high velocity phosphoprotein wave, which can propagate the signal at the velocity of 25μm/sec with the distance over 1cm.

This node activation property also plays an important role in the immune system in the vertebrates. There are two major immunity strategies (adaptive and innate) employed by the immune system in the vertebrates. In the adaptive immune system, the number of triggered T Cell Receptors (TCRs) determines when the T-cell will be activated. TCRs are triggered by ligands on the surface of antigen-presenting cells. When the number of the triggered TCRs reaches the threshold, the T-cell will be activated [23] [24] and then releases the signaling molecules, cytokines, to incur more immune responses. In the innate immune system, the node activation property is also observed in the Natural Killer (NK) cell. The receptors in NK cell can recognize the Major Histocompatibility Complex (MHC) I molecules on the surface of the normal cell. In the absence of the MHC I molecules in the infected cells, the NK cells will be activated to kill the cells with low MHC I molecules [25].

These three examples on existing neuron signal propagation and immune systems show that node activation plays an important role in the biological communication processes. To the best of our knowledge, our previous work in [26] is the first to address the node activation property in MNBOT networks. It shows that aggregation routing can help to satisfy node activation constraint. However, without capturing the Brownian motion interference in the high viscous biological fluids (e.g., urea or blood), the routing decisions might not

be applicable to bio-medical applications in low Reynolds number environment.

E. RESEARCH ON ROUTING

Routing has been an important issue in sensor networks that the data source nodes identify the energy efficient routing path to send the sensed data back to the sink node [35]. In wireless sensor networks (WSN) with stationary sink or mobile sink [36], aggregation routing strategy has been suggested to reduce the redundant information and wireless transmission power. Data aggregation strategy is especially useful in large networks with very large number of sensor nodes like IoT. A recent IoT study exploits the queuing delay for service aggregation to reduce the transmission volume and reduce the request response delay by using cache at the routers [37]. Considering the battery constraint in sensor node, battery-friendliness routing and relay node selection scheme has been proposed in [38] to prolong the lifetime for WSN.

Even though there are numerous existing researches on routing algorithms and protocols in WSN, these aggregation routing and relay node selection schemes are not applicable to the MNBOT routing in biological networks due to three reasons. First, the energy consumption in WSN comes from transmitting and receiving the wireless signal at the sensor nodes. In MNBOT networks, the energy consumption come from guiding the MNBOTs along the desired path. Second, the node activation property in biological processes is not addressed in the routing algorithms and protocols in WSN. Third, the existing researches in WSN do not address the Brownian motion interference in high viscous biological fluids.

The first in-vitro biological routing work appeared in [31] to guide and control the trajectory path of multiple MNBOTs via magnetic force. First node activation property aware MNBOT routing work appeared in [26], and it showed that aggregating MNBOTs on the routing path could help to activate the nodes on the routing path more efficiently. However, the interference from Brownian motion is not addressed in [26] to capture the MNBOT movement behavior in high viscous biological fluids.

In this paper, by leveraging on the aforementioned group MNBOT navigation scheme and MNBOT hardware technologies, we address the MNBOT routing scheme that captures the node activation property in existing biological communication processes. In addition, we propose a new optimization-based algorithm (LGA) that addresses the penalty cost from violating the node activation constraint. By considering the interplay between guiding force and Brownian motion, LGA algorithm identifies more efficient routing decisions than the three proposed heuristics in [26]. To summarize, we propose a node-activation-based and Brownian motion aware MNBOT routing scheme to propagate the biological signal in high viscous biological fluids more efficiently.

III. NODE ACTIVATION AND EMAR MODEL

The node activation property states that for any node on the routing path, it must be activated first before it can transmit MNBOTs with payloads to other nodes. The node activation property is formulated in Equation (1).

$$\Delta_i \leq \sum_{l \in L} M_l \, \sigma_{li} \tag{1}$$

In Equation (1), Δ_i indicates the received MNBOT threshold to activate node i; M_l indicates the number of MNBOTs on link l; σ_{li} is the indication function which is equal to 1 if node i is the terminating node on link l and $\sigma_{li} = 0$ if node i is not the terminating node on link l. Then the term $\left(\sum_{l \in L} M_l \, \sigma_{li}\right)$ calculates the number of received MNBOTs at node i. Equation (1) specifies the necessary condition of the node activation property that the received MNBOTs at a node must be no less than the activation threshold to activate a node.

Besides node activation constraint, node activation property also incurs a new molecular aware transmission problem. Unlike transmitting IP packets via electromagnetism in IP networks, molecular transportation via MNBOT in biological system has to convert the energy from the bio-chemical reaction between fuels and catalyst in the chamber of MNBOT into gas bubbles to generate the mechanical power to propel the MNBOT. Basically, transporting more MNBOTs will incur more transportation energy. Hence,

$$A_l = a_l \times M_l. \tag{2}$$

In Equation (2), a_l indicates the link cost to transport one MNBOT on link l. Then, A_l calculates the total cost to transport M_l number of MNBOTs on link l. Note that in the biological fluids (e.g., urea or blood) with low Reynolds number, the random movement of MNBOTs from Brownian motion should be carefully addressed [7]. The guiding force for MNBOTs are introduced to overcome the random movement from Brownian motion so that the MNBOT can reach the destination. In other words, the link cost of transporting an MNBOT (i.e., a_l) should take Brownian motion interference and guiding force into account.

$$a_l = \phi\left(\Theta_l, \Lambda_l, d_l\right). \tag{3}$$

In Equation (3), we define a_l as a function of guiding force (i.e., Θ_l), Brownian motion (i.e., Λ_l) and the Euclidean distance (i.e., d_l) on link l. In the computational experiments, we study this link cost with considering the Brownian motion in different levels of magnetic force guidance.

Based on node activation constraint and molecular aware cost as defined in Equations (1) and (2), node activation property introduces a new *Activation Based Molecular Routing* (*ABMR*) scheme in biological system which is different from existing Shortest path Based Routing (SBR) scheme in IP networks.

In Figure 2, we illustrate a bio-sensing application in which data source nodes sense and send the signaling molecules

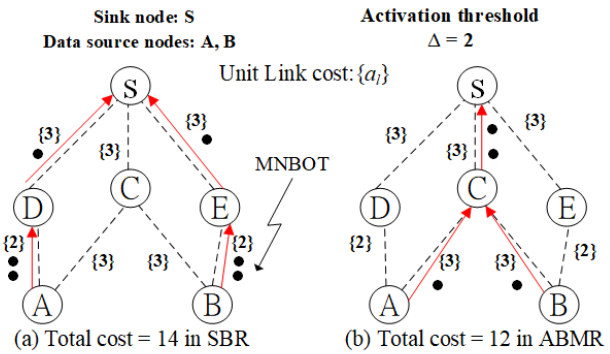

FIGURE 2. MNBOT routing in SBR and ABMR.

carried by MNBOTs back to the sink node. To realize the bio-sensing application in Figure 1, we assume that each node is attached with microscale MEMS-fabricated coils that can generate the local magnetic field as shown in [31]. In addition, each node is equipped with the computing module, storage and CNT communication module as indicated in Section I. By embedding CNT radio, each node communicates with other nodes to exchange the topology information and the information of node activation status. Based on the information, the sink node will compute and distribute the routing decisions to each node via wireless signal. Then, each node generates the magnetic field to attract or repel the MNBOTs based on the received routing decisions.

In Figure 2, the node action constraint has to be satisfied all the way from the data source nodes back to the sink node. In Figure 2(a), every data source node identifies the shortest path to the sink node via the SBR algorithm. By considering the node activation constraint to activate every node along the path, based on Equation (2), the total cost will be 14 (=2×2+3×1+2×2+3×1). However, a more cost-efficient routing is shown in Figure 2(b) where the MNBOTs are first aggregated at node C before transmitting to the sink node S. In this case, the total cost is 12 (=3×1+3×1+3×2).

To tackle the ABMR problem in bio-sensing applications, a mathematical model, called Efficient Molecular Activation and Routing (EMAR), is proposed. Efficiency is a very important design criterion in resource (i.e., MNBOTs) limited MNBOT networks. Note that "Efficient" in the EMAR model is to facilitate efficient molecular transporting and routing via MNBOTs in considering two properties (i.e., node activation constraint and molecular aware link cost) defined in Equations (1) and (2).

Before presenting the EMAR model, the notations used in the formulation are listed as follows.

Input values:
N: the set of nodes;
L: the set of links;
D: the set of data source nodes;
S: the set of sink node;
ρ_{li} : indication function, =1 if node i is the starting node of link l; =0, otherwise;
σ_{li} : indication function, =1 if node i is the terminating node of link l; =0, otherwise;
Δ_i : the received MNBOT threshold to activate node i;
d_l: the Euclidean distance of link l;
$\phi(\Theta_l, \Lambda_l, d_l)$: also denoted as a_l, is the unit cost of transmitting one MNBOT on link l, which is a function of guiding force (i.e., Θ_l), Brownian motion (i.e., Λ_l) and the Euclidean distance (i.e., d_l) on link l;
Ω_i : the MNBOT capacity at node i;
$\overline{\Omega}$: the MNBOT capacity upper bound, i.e., $\overline{\Omega} \geq \Omega_i \ \forall i \in N$;
Φ_i: be the set of incoming links into node i, i.e., $\sigma_{li} = 1 \ \forall l \in \Phi_i$;
Decision variables:
M_l: the number of MNBOTs transported on link l;
v_i: =1 if node i is activated; = 0, otherwise;

$$\text{Problem (P): } Z_{IP} = Min \sum_{l \in L} \phi(\Theta_l, \Lambda_l, d_l) M_l$$

Subject to:

$$v_i = 1 \qquad \forall i \in D \cup S \tag{4}$$

$$v_i \Delta_i \leq \sum_{l \in L} M_l \sigma_{li} \qquad \forall i \in N - S - D \tag{5}$$

$$\Delta_i \leq \sum_{l \in L} M_l \sigma_{li} \qquad \forall i \in S \tag{6}$$

$$0 < \sum_{l \in L} \rho_{li} M_l \qquad \forall i \in D \tag{7}$$

$$\sum_{l \in L} \rho_{li} M_l \leq v_i \Omega_i \qquad \forall i \in N \tag{8}$$

$$M_l \in \left\{0, 1, 2, \ldots, \bar{\Omega}\right\} \qquad \forall l \in L \tag{9}$$

$$v_i = 0 \text{ or } 1 \qquad \forall i \in N - D - S. \tag{10}$$

The objective function of Problem (P) is to minimize the total energy cost to propel MNBOTs to deliver the payloads to the sink node. Constraints (4) and (7) require that the data source nodes to be activated to transmit the sensed data via MNBOT back to the sink node. Constraint (5) requires that, besides the data source nodes and the sink node, if any node i is activated, then the received MNBOTs at node$i$ must be no less than threshold Δ_i. Constraint (6) enforces that the received MNBOTs at the sink node should be no less than the activation threshold, so that the sink node will be activated. Constraint (7) enforces that the data source node should choose at least one of its outgoing links to transmit MNBOTs. Hence, Constraints (5), (6) and (7) enforce the node activation constraint. Constraint (8) specifies the MNBOT capacity constraint where the total released MNBOTs from node i should not exceed the MNBOT capacity Ω_i at node i. Hence, Constraint (8) specifies the number of available MNBOTs at node i. Constraints (9) and (10) define the feasible regions of the decision variables $M_l$andv_i.

Note that Constraint (7) is to enforce the sending of signaling molecules at each data source node. Without including Constraint (7) in Problem (P), some of the data source nodes

may not send the signaling molecules back to the sink node so that events (e.g., infected cells response in innate immune system) cannot be detected and responded. Hence, in biosensing applications, it is essential to enforce Constraint (7) to make sure every data source node senses the event and sends the signaling molecules back to the sink node.

Besides the two properties (node activation constraint and molecular aware link cost) in ABMR, Problem (P) also captures the MNBOT capacity constraint (i.e., the resource constraint of available MNBOTs) at Constraint (8). Hence, Problem (P) captures the three properties (i.e., molecular aware link cost, node activation property and MNBOT capacity constraint) of ABMR in resource limited MNBOT networks.

EMAR is a generic model to capture the node activation property in the biological processes. Let us consider applying EMAR model to a specific application on the immune system dealing with virus infected cells without MHC I molecules. In this example, we assume that a node has the capability of detecting the virus infected cells without MHC I molecules. When detecting the virus infected cells, the data source nodes will release the MNBOTs that carry signaling molecules (i.e., cytokines) to activate the immune cells (i.e., NK cells) or other nodes for triggering more immune responses. Enforcing three characteristics of ABMR in the constraints, the EMAR model identifies efficient and effective molecular routing scheme to activate and proliferate the immune response against the virus infected cells (i.e., to activate more NK cells for attacking the virus infected cells).

Before we present the algorithm to tackle Problem (P), we show that Problem (P) is an NP-hard problem. In Problem (P), Δ_i determines the MNBOT threshold to activate node$i$. If we set $\Delta_i = 1\ \forall i \in N$(i.e., no node activation constraint), then Problem (P) identifies the paths for every data source node back to the sink node with the minimum cost of the selected links. In the undirected network where the link cost on both directions is the same, Problem (P) identifies the minimum cost multicast tree from the sink node to all the data source nodes. For example, in Figure 2, when activation threshold $\Delta = 1$, the total cost is 9 (the routing assignment of Problem (P) is shown in Figure 2(b)), which is the same as the minimum multicast tree from the sink node S to the data source nodes$A$ and B. In other words, Problem (P) will be reduced to the minimum cost multicast tree when there is no node activation constraint. Since the minimum cost multicast tree is a Steiner tree problem, which is proven to be an NP-hard problem [27], then Problem (P) is also an NP-hard problem.

In the sequel, we devise the algorithm based on the Lagrangian relaxation method to tackle the problem (P).

IV. SOLUTION APPROACHES– LAGRANGIAN RELAXATION

A. LAGRANGIAN DUAL PROBLEM

The algorithm development is based upon Lagrangian relaxation. In (P), by introducing Lagrangian multiplier vector μ_i, we dualize Constraints (5), (6), (8) to obtain the following Lagrangian relaxation problem (LR).

Problem (LR):

$$Z_{LR}(\mu_i) = \text{Min} \sum_{l\in L} \phi\left(\Theta_l, \Lambda_l, d_l\right) M_l + \sum_{i\in N-S-D} \mu_i^1 \left(v_i\Delta_i - \sum_{l\in L} M_l\sigma_{li}\right) + \sum_{i\in S} \mu_i^2 \left(\Delta_i - \sum_{l\in L} M_l\sigma_{li}\right) + \sum_{i\in N} \mu_i^3 \left(\sum_{l\in L} \rho_{li}M_l - v_i\Omega_i\right)$$

Subject to:

$$v_i = 1 \qquad \forall i \in D \cup S \tag{11}$$

$$0 < \sum_{l\in L} \rho_{li}M_l \qquad \forall i \in D \tag{12}$$

$$M_l \in \left\{0, 1, 2, \ldots, \bar{\Omega}\right\} \qquad \forall l \in L \tag{13}$$

$$v_i = 0 \text{ or } 1 \qquad \forall i \in N - D - S. \tag{14}$$

Problem (LR) can be decomposed into two independent subproblems which are associated withM_l and v_i.

Subproblem 1: forM_l

$$\min \sum_{l\in L} \phi\left(\Theta_l, \Lambda_l, d_l\right) M_l + \sum_{l\in L} \left(\left(\sum_{i\in N} \mu_i^3\rho_{li}\right) - \left(\sum_{i\in N-S-D} \mu_i^1\sigma_{li}\right) - \left(\sum_{i\in S} \mu_i^2\sigma_{li}\right)\right) M_l \tag{SUB1}$$

subject to (12) and (13).

Subproblem 2: for v_i

$$\text{Min} \sum_{i\in N-S-D} \left(\mu_i^1\Delta_i - \mu_i^3\Omega_i\right) v_i - \sum_{i\in S\cup D} \left(\mu_i^3\Omega_i\right) v_i + \sum_{i\in S} \mu_i^2\Delta_i \tag{SUB2}$$

subject to (11) and (14).

In the Constraint (12) of (SUB1), they enforce that at least one outgoing link should be selected for each data source node. Then (SUB1) can be decomposed into $|N|$ independent subproblems where each subproblem deals with the set of outgoing links from each node. Let Γ_j be the set of outgoing links from node j. To successfully tackle (SUB1), we consider the node j in three cases, which are $j \in D, j \in S$ and $j \in N - S - D$.

Case 1: node j is the data source node (i.e., $j \in D$).

In case 1, consider each subproblem of (SUB1) with respect to node $j \in D$,

$$\text{Min} \sum_{l\in\Gamma_j} \left(\phi\left(\Theta_l, \Lambda_l, d_l\right) - \sum_{i\in N-S-D} \mu_i^1\sigma_{li} - \sum_{i\in S} \mu_i^2\sigma_{li} + \mu_j^3\right) M_l \tag{SUB1-1}$$

subject to

$$0 < \sum_{l \in \Gamma_j} M_l \tag{15}$$

$$M_l \in \left\{0, 1, 2, \ldots, \bar{\Omega}\right\} \qquad \forall l \in \Gamma_j. \tag{16}$$

Case 2: node j is the sink node (i.e., $j \in S$).
In case 2, consider each subproblem of (SUB1) with respect to node $j \in S$,

$$\underset{M_l}{\text{Min}} \sum_{l \in \Gamma_j} \left(\phi\left(\Theta_l, \Lambda_l, d_l\right) - \sum_{i \in N-S-D} \mu_i^1 \sigma_{li} - \sum_{i \in S} \mu_i^2 \sigma_{li} + \mu_j^3 \right) \qquad \text{(SUB1-2)}$$

subject to

$$M_l \in \left\{0, 1, 2, \ldots, \bar{\Omega}\right\} \qquad \forall l \in \Gamma_j. \tag{17}$$

Case 3: node j is the none-data source node and none-sink node (i.e., $j \in N - S - D$).
In case 3, consider each subproblem of (SUB1) with respect to node $j \in N - S - D$,

$$\underset{M_l}{\text{Min}} \sum_{l \in \Gamma_j} \left(\phi\left(\Theta_l, \Lambda_l, d_l\right) - \sum_{i \in N-S-D} \mu_i^1 \sigma_{li} - \sum_{i \in S} \mu_i^2 \sigma_{li} + \mu_j^3 \right) \qquad (SUB1-3)$$

subject to

$$M_l \in \left\{0, 1, 2, \ldots, \bar{\Omega}\right\} \qquad \forall l \in \Gamma_j. \tag{18}$$

In (SUB1), for each outgoing link$l$ from node j, the arc weight associated with M_l is calculated in Equation (19).

$$\text{Arc weight of } M_l = \left(\phi\left(\Theta_l, \Lambda_l, d_l\right) - \sum_{i \in N-S-D} \mu_i^1 \sigma_{li} - \sum_{i \in S} \mu_i^2 \sigma_{li} + \mu_j^3 \right) \quad \forall l \in \Gamma_j, j \in N \tag{19}$$

In (SUB1-1), since at least one MNBOT should be transmitted from data source node j, then we first calculate the arc weight in Equation (19) for each outgoing link from node j. If at least one outgoing link has negative arc weight, assign $M_l = \bar{\Omega}$ for those outgoing links with negative arc weight, otherwise assign $M_l = 1$ for the outgoing link with smallest arc weight. With these optimal decision variable settings on M_l, the smallest objective function in (SUB1-1) could be obtained.

In (SUB1-2), one might think that the sink node is the destination node so that no MNBOTs will be transported out from the sink node. Hence, $M_l = 0, \forall l \in \Gamma_i, i \in S$. However, in the general case, when there are multiple sink nodes in set S, it is possible to transport the MNBOTs on the outgoing links from a sink node to the other sink nodes. In this case, $M_l > 0, \forall l \in \Gamma_i, i \in S$. Then the optimal solution procedure to solve (SUB1-2) is as follows. Let $M_l = \bar{\Omega}$ when the associated arc weight in Equation (19) is negative and let $M_l = 0$ when the associated arc weight in Equation (19) is not negative for each outgoing link l from node j.

In (SUB1-3), we deal with the outgoing links from node j that is a none-data source node and none-sink node. The optimal solution procedure to solve (SUB1-3) is as follows. Let $M_l = \bar{\Omega}$ when the associated arc weight in Equation (19) is negative and let $M_l = 0$ when the associated arc weight in Equation (19) is not negative for each outgoing link l from node j.

The algorithm to optimally solve (SUB1) is shown below. The computational complexity for the following algorithm is $O(|N| \cdot |L|)$.

In (SUB2), there are two settings of the arc weight associated with v_i as follows.

$$\text{Arc weight of } v_i = \left(\mu_i^1 \Delta_i - \mu_i^3 \Omega_i\right) i \in N - S - D \tag{20}$$

$$\text{Arc weight of } v_i = \left(-\mu_i^3 \Omega_i\right) i \in S \cup D. \tag{21}$$

In the case of $i \in N - S - D$, calculate the arc weight $\left(\mu_i^1 \Delta_i - \mu_i^3 \Omega_i\right)$ as shown in (20). If the coefficient is negative, let $v_i = 1$, otherwise let $v_i = 0$. On the other hand, in the case of $i \in S \cup D$, because of Constraint (11), let $v_i = 1\ i \in S \cup D$. The computational complexity of (SUB2) is $O(|N|)$.

Based on the above algorithms to solve (SUB1) and (SUB2), we can solve the Lagrangian dual problem (LR) optimally. Based on the Lagrangian duality theorem, the solutions to the (LR) problem is a legitimate lower bound to the primal problem (P). By the weak duality theorem [27], given any nonnegative multiplier, Z_{LR} is a lower bound to Z_{IP}. We can use subgradient method to calculate the tightest lower bound [27], Z_D, as shown below.

$$\text{Problem (D): } Z_D = \text{Max } Z_{LR}\left(\mu_i^1, \mu_i^2, \mu_i^3\right)$$

$$\text{Subject to: } \mu_i^1, \mu_i^2, \mu_i^3 \geq 0$$

Let the vector S be a subgradient of $Z_{LR}\left(\mu_i^1, \mu_i^2, \mu_i^3\right)$ at $\left(\mu_i^1, \mu_i^2, \mu_i^3\right)$. In iteration x of the subgradient optimization procedure, the multiplier vector $m_x = \left(\mu_{i^1}^1, \mu_{i^2}^2, \mu_{i^3}^3\right)$ is updated by $m_{x+1} = m_x + \alpha^x S^x$, where $S^x\left(\mu_i^1, \mu_i^2, \mu_i^3\right) = \left(v_i \Delta_i - \sum_{l \in L} M_l \sigma_{li}, \Delta_i - \sum_{l \in L} M_l \sigma_{li}, \sum_{l \in L} \rho_{li} M_l - v_i \Omega_i\right)$.

The step size $\alpha^x$is determined by $\left(\delta \frac{Z_{IP}^h - Z_{LR}(m^x)}{\|S^x\|^2}\right)$, where Z_{IP}^h is a primal objective function value (an upper bound on optimal primal objective function value), and δ is a step size coefficient ($0 \leq \delta \leq 2$).

B. GETTING PRIMAL SOLUTIONS – LRP

In the following, we will use the information from the solutions and the multipliers at the (LR) to derive the primal heuristic algorithm to get the feasible solution for the original problem (P).

We propose getting primal heuristic algorithm – LRP algorithm, to solve problem (P). LRP adopts the idea of Dijkstra's shortest path algorithm where the *molecular aware cost to activate the link's termination node* is set as the link arc

Algorithm to optimally solve (SUB1)
Begin
For $(j = 1; j <= |N|; j++)$
Begin
Let $M_l = 0, \forall l \in \Gamma_j$; //initialization
If $(j \in D)$ //Data source nodes
Begin
Calculate the link arc weight $\left(\phi(\Theta_l, \Lambda_l, d_l) - \sum_{i \in N-S-D} \mu_i^1 \sigma_{li} - \sum_{i \in S} \mu_i^2 \sigma_{li} + \mu_j^3\right)$ of $M_l \forall l \in \Gamma_j$;
Let Ψ_i be the number of links with negative arc weight;
If $(\Psi_i = 0)$
Identify an outgoing link l with the smallest arc weight and assign $M_l = 1$;
Else
Identify the outgoing links with the negative arc weight and assign $M_l = \bar{\Omega}$ for those outgoing links;
End// If $(j \in D)$
If $(j \in S)$ //sink node
Begin
For $(\forall l \in \Gamma_j)$
Begin
If $\left(\phi(\Theta_l, \Lambda_l, d_l) - \sum_{i \in N-S-D} \mu_i^1 \sigma_{li} - \sum_{i \in S} \mu_i^2 \sigma_{li} + \mu_j^3 < 0\right)$
$M_l = \bar{\Omega}$;
Else
$M_l = 0$;
End//for
End//$j \in S$
If $(j \in N - S - D)$ //other nodes
Begin
For $(\forall l \in \Gamma_j)$
Begin
If $\left(\phi(\Theta_l, \Lambda_l, d_l) - \sum_{i \in N-S-D} \mu_i^1 \sigma_{li} - \sum_{i \in S} \mu_i^2 \sigma_{li} + \mu_j^3 < 0\right)$
$M_l = \bar{\Omega}$;
Else
$M_l = 0$;
End//for
End//$j \in N - S - D$
End //For j
End

weight. We first calculate the number of MNBOTs needed to be transported on link$l$ for node activation in Equation (22).

$$f_l^n = Min\left\{\left(\sum_{i \in N} \Omega_i \rho_{li}\right), \sum_{i \in N} (\Delta_i - \lambda_i)\sigma_{li}\right\} \forall l \in L \quad (22)$$

Note that the adopted Lagrangian relaxation process is an iteration-based approach to get better solutions in problem (P). The complete iteration-based algorithm to solve primal problem (P) and dual problem (LR) is shown at the end of the Section IV. Using the information from earlier iteration, in Equation (22), f_l^n calculates the number of newly transported MNBOTs on link l. $\lambda_i$indicates the received MNBOTs on this node i at the earlier iteration in the Lagrangian relaxation process. $\sum_{i \in N} \Omega_i \rho_{li}$ calculates the MNBOT capacity constraint at link l's starting node; $\left(\sum_{i \in N} (\Delta_i - \lambda_i)\sigma_{li}\right)$ calculates the number of MNBOTs needed on link l so as to activate link l's terminating node i. The minimum value of $\left\{\sum_{i \in N} \Omega_i \rho_{li}, \sum_{i \in N} (\Delta_i - \lambda_i)\sigma_{li}\right\}$ is to make sure that the MNBOTs assignment on link $l$will satisfy the node activation constraint at the link's termination node and MNBOT capacity constraint at the link's starting node simultaneously.

$$\eta_i = \underset{l \in \Phi_i \wedge M_l > 1}{\text{Arg}} \; Max\left(\phi(\Theta_l, \Lambda_l, d_l)\right) \qquad \forall i \in N \quad (23)$$

$$\beta_l = \left(f_l^n - f_l^o\right) \times \left(\phi(\Theta_l, \Lambda_l, d_l) + \mu_i^1 - v_i \times \phi\left(\Theta_{\eta_i}, \Lambda_{\eta_i}, d_{\eta_i}\right)\right) \qquad \forall l \in \Phi_i, i \in N - D - S \quad (24)$$

Or

$$\beta_l = \left(f_l^n - f_l^o\right) \times \left(\phi(\Theta_l, \Lambda_l, d_l) + \mu_i^2 - v_i \times \phi\left(\Theta_{\eta_i}, \Lambda_{\eta_i}, d_{\eta_i}\right)\right) \qquad \forall l \in \Phi_i, i \in S \quad (25)$$

Or

$$\beta_l = \left(f_l^n - f_l^o\right) \times \phi(\Theta_l, \Lambda_l, d_l) \qquad \forall l \in \Phi_i, i \in D. \quad (26)$$

In Equation (23), $\Phi_i$is the set of the incoming links to node i and $M_l > 1$ indicates that at least 2 MNBOTs are transported on link l. Then, $\eta_i$identifies the link with the largest unit MNBOT transmission cost that have already transported at least 2 MNBOTs among the incoming links to node i. The reason that we need to enforce $M_l > 1$ in Equation (23) is because one MNBOT is going to be removed from link l at Equations (24)∼(26).

We next calculate the activation aware link cost metric β_l of link l in Equations (24)∼(26). In Equations (24)∼(26), f_l^o indicates the original number of MNBOTs on link l. In Equations (24)∼(26), the term $\left(f_l^n - f_l^o\right)$ calculates the new admitted number of MNBOTs on link l. The second term in Equations (24)∼(26) calculates the modified unit MNBOT transmission cost. This modified MNBOT transmission cost captures the original unit MNBOT transmission cost, the penalty cost for violating the node activation constraint and the gain from removing one MNBOT from other links with the largest unit MNBOT transmission cost that has the same termination node as link l.

Note that in the Lagrangian relaxation scheme, the Lagrangian multipliers imply the penalty cost for violating the relaxed constraint. When the node activation property constraint is violated, the value of the associated multiplier μ_i^1 and μ_i^2 will be increased at the next iteration. By incorporating these multipliers into the arc weight, the data source node will avoid choosing the link with high activation cost to activate the link's termination node in the previous

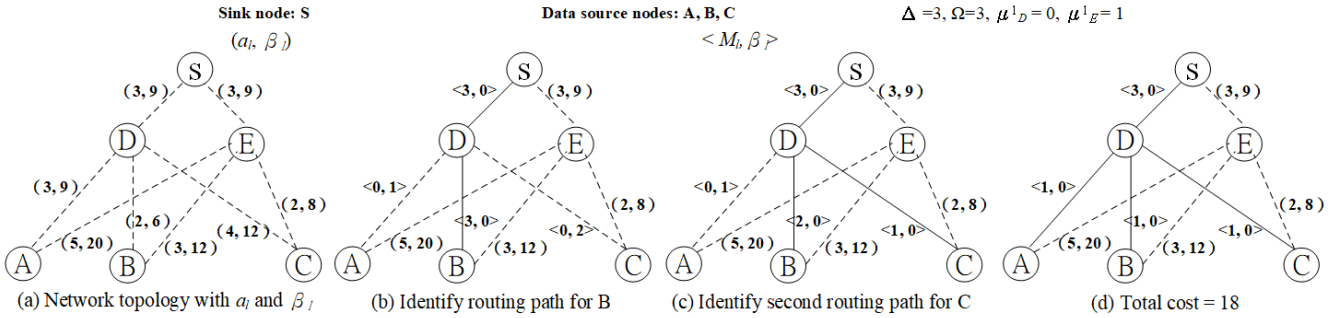

FIGURE 3. Illustrative example of LRP algorithm.

Lagrangian iteration. As we will show in the computational experiments, introducing the Lagrangian multipliers into the link cost metric can help to identify more energy efficient paths.

In LRP algorithm, the activation aware link cost metric β_l is used in the Dijskstra's algorithm to determine the routing path for each data source node. Because of the node activation constraint, the sequence order of identifying the routing path for the data source nodes plays an important role in determining the final MNBOT transmission cost. For example, in Figure 3, the sequence order of identifying routing path for data source nodes is from node B then node C and finally node A. In this case, the total MNBOT routing assignment cost is 18. If the sequence order becomes C, B and A, then the routing paths will be aggregated at node E and total MNBOT routing assignment cost is 19.

Based on this observation, the basic idea is to start with the data source node with lower MNBOT transmission cost and then encourage other data source nodes to transmit MNBOTs on existing path to reduce the total MNBOT transmission cost. As shown at step 3 and step 4 in the LRP algorithm, set Π contains the elements of data source nodes where the sequence order of the elements is determined by MNBOT transmission cost to the sink node in ascending order. Hence, in Figure 3, $\Pi = \{B, C, A\}$. By selecting one data source node from set Π at a time to identify the routing path to the sink node, remaining unvisited data source nodes with higher transmission cost in set Π will be encouraged to identify the routing path on existing established routing path to save the total MNBOT transmission cost.

In assigning the molecules on the routing path for each data source node, when $f_l^n = 0$, it indicates that the termination node of link l is already activated so that there is no need to assign MNBOTs on link l. However, Constraint (7) requires that each data source node should at least transmit one MNBOT along its routing path to the sink node. Therefore, we transmit one MNBOT from the link l's starting node. When transmitting one more MNBOT on link l, one MNBOT can be reduced at one of the other incoming links that has the same termination node as link l. As shown in step 11 in LRP algorithm, by choosing the incoming link η_i as shown at Equation (23), the objective function in problem (P) can further be reduced by deducting the value of $\phi\left(\Theta_{\eta_i}, \Lambda_{\eta_i}, d_{\eta_i}\right)$.

The computational complexity for the LRP algorithm is determined by the nested "For" loop to identify the routing and molecular assignment for each data source node (i.e., step 3). Inside the nested "For" loop, in Step 8, the time complexity is $O(|L|)$. The number of data source node is $|D|$, and the number of selected links by a data source node is at most $(|L|)$. So, the iterations of the nested "Loop" loop is $O(|D| \cdot |L|)$ times. Then, the time complexity for the nested "For" loop is $O(|D| \cdot |L|^2)$. The time complexity of LRP algorithm is also $O(|D| \cdot |L|^2)$.

Basically, LRP is a link state routing protocol, in which each node will periodically broadcast the information of its incident links (i.e., a_l) and node information (i.e., Δ_i and Ω_i) on the network. In addition, LRP is a centralized algorithm that after collecting the link and node information from all the nodes, the sink node will compute and disseminate the routing information to other nodes in the networks.

An illustrative example of LRP algorithms is shown in Figure 3. We have the set $\Pi = \{B, C, A\}$ based on this path cost by using the Dijkstra's shortest path algorithm in Figure 3(a). In Figure 3(b), it shows the results after assigning the number of transmitted MNBOTs on the routing path B and before assigning the number of transmitted MNBOTs on the routing path for C. Based on Equation (22), the MNBOTs assignment are all 3 on link BD and link DS so that nodes D and S are all activated. In Figure 3(b), to calculate the link arc weight on link AD as shown in Equation (25), $\beta_l = (1 - 0) \times (3 + 0 - 2) = 1$. Likewise, the link arc weight on link CD, $\beta_l = (1 - 0) \times (4 + 0 - 2) = 2$.

In Figure 3(c), when the MNBOTs assignment for data source node C is performed, we first get $f_{CD} = 0$. In this case, we still need to assign one MNBOT on link CD to satisfy the routing path constraint for data source node C. Based on step 10 in LRP algorithm, we assign one MNBOT on link CD. According to step 11, to satisfy the node activation constraint node D, we can reduce one MNBOT on link BD so that it only needs to transmit two MNBOTs. Note that after assigning one MNBOT on link CD, the β_l is still 1 on link AD. This is because even though $a_{CD} > a_{BD}$, $M_{CD} > 1$ requirement in Equation (23) is not satisfied (i.e., $M_{CD} = 1$). Hence, after the MNBOT assignment on the routing path for node A, the final MNBOT and routing assignment is shown at Figure 3(d).

LRP algorithm
Begin
For $\forall l \in L$
Begin
Compute f_l^n and η_i in Equations (22), (23);//step 1
Compute β_l in Equations (24)∼(26);//step 2
End
Perform Dijkstra's shortest path algorithm for each data source node based on the link arc weight β_l; //step 3
Sorting path cost for all data source nodes in ascending order and put these data source nodes in set Π; //step 4
For data source node $j \in \Pi$ //step 5
Begin
For $\forall l \in L$
Begin
Compute f_l^n and η_i in Equations (22), (23);//step 6
Compute β_l in Equations (24)∼(26);//step 7
End
Perform the Dijkstra algorithm to determine the routing path for data source node$j$; //step 8
For each link$l$ selected by node$j$// step 9
Begin
i= link l's termination node;
If ($f_l^n == 0$)//link l's termination node already activated
Begin
$f_l^n = 1$; //step 10, assign one MNBOT on link l
$f_{\eta_i}^n = f_{\eta_i}^n - 1$; //step 11, deduct one MNBOT on link η_i
End//If f_l^n
Else// $f_l^n > 0$, check if link l's termination node is activated
Begin
$\lambda_i = \lambda_i + f_l^n$;//step 12
If ($\lambda_i == \Delta_i$)//activation constraint satisfied at node i
$v_i = 1$; //step 13
End//Else
$M_l = f_l^n$;
$f_l^o = f_l^n$;
End//For l, end of step 9
End//For j, end of step 5
If the activation capacity constraint is violated
Report infeasible solutions;
Else
Report total molecular transmission cost;
End//If
End

Note that the link cost (i.e., $\phi(\Theta_l, \Lambda_l, d_l)$) indicates the cost of moving one MNBOT on the link l. When applying the external force, like magnetic force, the link cost is set to deploy the magnetic field to guide transmitted MNBOTs on the link l. Then the objective function is to minimize the total magnetic force deployment cost on the MNBOT

LGA algorithm
Begin
Read input values of given parameters in Problem (P);
Initialize the Lagrangian multiplier vector $(\mu_i^1, \mu_i^2, \mu_i^3)$ to be all zero vector;
UB:= $\left(\sum_{l \in L} \phi(\Theta_l, \Lambda_l, d_l) \cdot \bar{\Omega}\right)$; LB:= 0;
quiescence_age:= 0; step_size_coefficient:= 2;
For x:= 1 to Max_Iteration_Number do
Begin
RUN algorithm to solve (SUB1);
RUN algorithm to solve (SUB2);
Calculate Z_{LR};//the dual objective value in problem (LR)
if $Z_{LR} >$ LB then
LB:= Z_{LR}; quiescence_age:= 0;
Else quiescence_age:= quiescence_age + 1;
If quiescence_age == Quiescence_Threshold then
quiescence_age:= 0; and $\delta := \left(\delta/2\right)$;
$f_l^o = 0, \forall l \in L$; $\lambda_i = 0, \forall i \in N$; //initialized
Run LRP algorithm to get the primal feasible solution Z_{IP}^h; //the objective value in problem (P)
If $Z_{IP}^h <$ UB then UB:= Z_{IP}^h; // found a tighter upper bound $S^x\left(\mu_i^1, \mu_i^2, \mu_i^3\right) := \left(v_i\Delta_i - \sum_{l \in L} M_l\sigma_{li}, \Delta_i - \sum_{l \in L} M_l\sigma_{li}, \sum_{l \in L} \rho_{li}M_l - v_i\Omega_i\right)$;//
calculate subgradients of the multipliers $\alpha^x = \left(\delta \frac{Z_{IP}^h - Z_{LR}(m^x)}{\|S^x\|^2}\right)$; //update step size, $m_{x+1} = m_x + \alpha^x S^x$; //update Lagrangian multipliers
End;//For
End;//LGA

travelled distance. With this link cost setting, the LRP algorithm identifies the guiding force efficient MNBOT transportation plan.

To summarize, in the LRP algorithm, the basic idea is to encourage MNBOT aggregation at the relay nodes that can save the total MNBOT transmission cost with considering the node activation constraint. In addition, the routing algorithm based on link arc weight metric β_l captures the interplay between unit MNBOT transmission cost, node activation constraint and MNBOT capacity constraint simultaneously to minimize the total MNBOT transmission cost.

In the following, we show the complete algorithm, Lagrangian Algorithm (LGA), to solve the primal Problem (P) and Lagrangian dual Problem (LR).

The computational complexity for LGA is $O(|D| \cdot |L|^2)$ for each iteration.

V. COMPUTATIONAL EXPERIMENTS

A. MAGNETIC GUIDANCE COST WITHOUT BROWNIAN MOTION

In the computational experiments, we simulate the bio-activation-based communication scheme in a bio-sensor

network where 100 nodes are randomly deployed in a 25×25 mm^2 area where the top left corner is (0, 0) and the bottom right corner is (25, 25). The sink node is located at the top left corner (0, 0). Data source nodes are randomly selected from 100 nodes. The data source nodes will sense, collect and transmit the MNBOTs with signaling molecules as the payload to propagate the bio-signal all the way to activate the sink node in the bio-sensor network. Note that for all the nodes on the routing path from the data source nodes to the sink node, node activation property is enforced. Hence, every node must be activated first before it can transmit MNBOTs with signaling molecules to activate the next node on the routing path. We perform the following computational experiments on the NS3 platform.

For LGA algorithm, Max_Iteration_Number and Quiescence_Threshold are set to 1000 and 30 respectively. The step size coefficient (δ) is initialized as 2 and is halved when the objective function value of the dual problem is not improved by iterations up to Quiescence_Threshold. The computational time is within seconds for LPR algorithm and within minutes for LGA algorithm.

The MNBOT movement parameters are adopted from a recently biocompatible microcapsule implementation in [28]. In [28], an MNBOT is built based on Janus hollow mesoporous silica microparticles and the hollow capsule can carry small molecules up to hundreds of nanometers. The MNBOT propulsion force comes from the biocatalytic reaction on the coating of the MNBOT with the biological fluids – urea into CO_2 and NH_3. In [28], the velocity of an MNBOT can reach 5 body length ($\sim$10 μm/sec) and the lifetime of an MNBOT can last 10 minutes. Then, the longest travelled distance for an MNBOT is 6 milli-meter. Considering the MNBOT lifetime constraint, in the simulated biosensor networks with 100 nodes, a link between two nodes is established if the distance is not greater than 6 mm in a 25×25 mm^2 deployment area.

The MNBOT orientation is guided by the external magnetic field with a strength 100 milli-Tesla in [28]. The cost of setting up the magnetic field on the link$l$ is proportional to the magnetic field strength and the distance on the link l. Based on this argument, the link cost metric to transmit an MNBOT on the link l (i.e., a_l) is set as the magnetic flux density in Tesla times the link Euclidean distance in meters. Hence, $a_l = 0.1d_l$ (Tesla $\times$ meter), where d_l is the Euclidean distance on link l. With this link arc weight setting, the objective function in Problem (P) at Section II aims to minimize the total magnetic guiding cost to guide all the MNBOTs on the routing path to the sink node in the bio-sensor networks.

In Figure 4, we show the solution quality in terms of the magnetic guiding cost between the proposed LGA algorithm and the other three heuristics, CACAMA, MCST and SPT that are proposed in our previous work [26]. Note that the proposed CACAMA algorithm in our previous work encourages molecular aggregation to save cost but it does not address the penalty from violating the node activation constraint. MCST is a minimum cost spanning tree approach to identify the minimum cost spanning tree for the data source nodes via the Prim's algorithm. SPT is a shortest path approach to identify the routing path from every data source node via the Dijkstra's shortest path algorithm. Note that in MCST and SPT, the link arc weight is also set as $a_l = 0.1d_l$. For these three approaches in [26], after the routing assignment is determined, we assign the MNBOTs on the selected links so that all the constraints in Problem (P) can be satisfied.

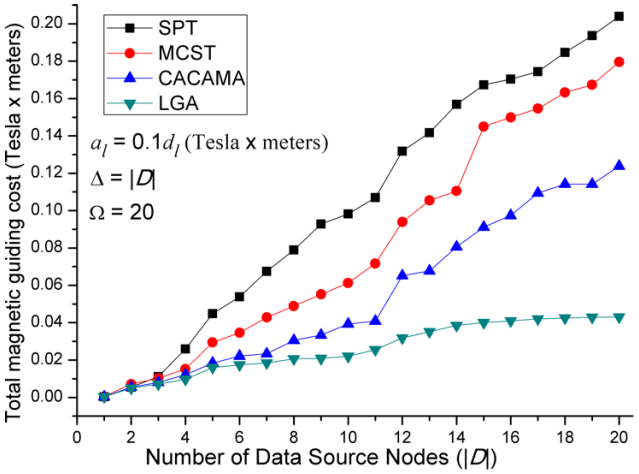

FIGURE 4. Total magnetic guiding cost (Tesla x meters) w.r.t. $|D|$.

In Figure 4, the node activation threshold is set as the number of data source nodes (i.e., $\Delta = |D|$). With this setting, by increasing the value of the data source nodes, the node activation threshold will also be increased. Intuitively, increasing the data source nodes means more MNBOTs should be transmitted to activate the nodes on the routing path, and this will increase the total magnetic guiding cost. As observed in Figure 4, by increasing the value of data source nodes, the total magnetic guiding cost increases more significantly for SPT, MCST and CACAMA algorithms than LGA algorithm. When $|D| = 20$, the total magnetic guiding cost saving for LGA over SPT, MCST and CACAMA are 374%, 317% and 188%, respectively. It shows that LGA algorithm facilitates better molecular aggregate strategy in considering the node activation constraint, especially at high traffic demands (i.e., large number of data source nodes).

In Figure 4, the link cost metric, a_l, only considers the link Euclidean distance on link l. As indicated in Section II, Brownian motion is non-negligible in biological fluids environment with low Reynolds number. Then the MNBOT travelled distance is longer than the Euclidean distance. In the next computational experiments, we study the MNBOT moving behavior in considering the impact from Brownian motion.

B. INTERPLAY OF BROWNIAN MOTION AND MAGNETIC GUIDANCE

Note that Brownian motion can be modeled by a continuous-time Wiener process. Let W_u be a random variable in the Wiener process that indicates the position of the MNBOT at time u. Then the difference between current position at time u

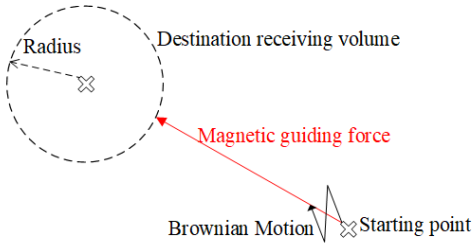

FIGURE 5. Interplay between Brownian motion and magnetic guidance.

and next position at time v follows a Normal distribution [29]. Hence,

$$W_v - W_u \sim \mathcal{N}(0, v-u)\ 0 \le u \le v \tag{27}$$

In Equation (27), it states that without any external force, an MNBOT moves randomly in fluids that follows a Normal distribution with zero mean. When guided by the magnetic force, an MNBOT moves fluctuated along the trajectory of the magnetic force as shown in Figure 5. The destination receives the MNBOT when the MNBOT move into the destination receiving volume. Because of the movement fluctuation, an MNBOT may not be able to reach the destination when the receiving volume is small.

In the following computational experiments, we set the radius of the receiving volume to be 10 micrometers, which is the about the size of lymphocytes (i.e., T cell, B cell and NK cell) in the human's immune system [30]. Based on this radius setting, we can examine if the design scheme could be applied to the immune system. To be more specific, we want to know if the MNBOT network can help the molecular activation process in lymphocytes to incur more immune responses against abnormal cells, bacteria and virus.

Basically, an MNBOT that moves in biological fluids might sometimes not be guided by the magnetic field because the magnetic force is not strong enough at some particular places. In this case, an MNBOT will move in a Brownian motion until the magnetic force is strong enough to guide the MNBOT again. In the next experiment, we study the MNBOT propagation delay under different percentages of the magnetic guidance with the consideration of the interplay between magnetic field and Brownian motion as shown in Figure 6.

In Figure 6, the MNBOT propagation delay results are shown from 20% to 100% magnetic guidance. Note that, 0% magnetic guidance (i.e., 100% Brownian motion) is not included in Figure 6 because the MNBOT cannot reach the destination receiving volume within 1 hour (3600 seconds) of simulation time even at the distance of 0.5 milli-meters. This movement fluctuation from Brownian motion interferes MNBOTs for reaching the destination with small receiving volume. This indicates that diffusion based MNBOT routing is not suitable for high precision bio-medical applications.

In Figure 6, we can observe that the MNBOT propagation delay increases as the percentage of Brownian motion increases. In addition, the MNBOT propagation delay with lower degree of magnetic force guidance increases more

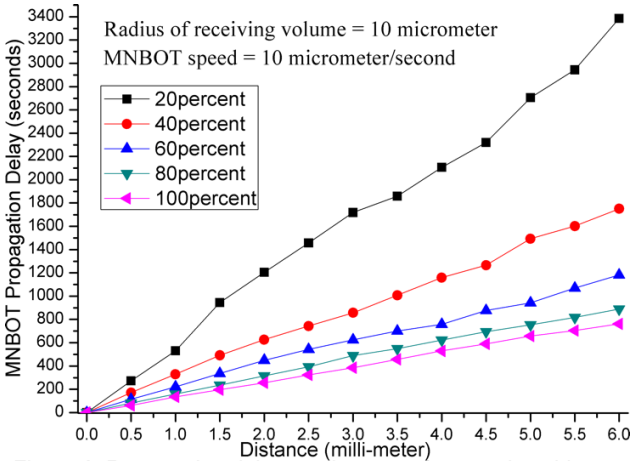

FIGURE 6. Propagation delay vs. degrees of magnetic guidance.

rapidly than MNBOT with higher degree of magnetic force guidance. This is because the MNBOT travelled distance is longer than the Euclidean distance between the two nodes considering the Brownian motion effect. That is, let d_l be the Euclidean distance on link l andt_l be the MNBOT travelled distance on link l, then $t_l > d_l$ when there is a Brownian motion effect. Then, with considering the 10 minutes MNBOT lifetime, the largest Euclidean distance between the two nodes that an MNBOT can travel is smaller than 6 mm. In Figure 6, it shows that with considering the Brownian motion effect and MNBOT lifetime, the largest Euclidean distance between two nodes for an MNBOT to travel is 4.5 mm, 3.5 mm, 2.5 mm, 1.5 mm, 1 mm under 100%, 80%, 60%, 40% and 20% magnetic guidance, respectively.

Based on the observations and results in Figure 6, we compare the solution quality of four routing schemes under 100 percent magnetic force guidance to enable MNBOT in high precision bio-medical applications. That is, in the simulated biosensor networks with 100 nodes, a link between two nodes is established if the Euclidean distance is not greater than 4.5 mm in a 25×25 mm^2 deployment area based on the results in Figure 6 that considers the MNBOT 10 minutes lifetime.

C. PERFORMACE COMPARISON IN CONSIDERING BROWNIAN MOTION AND MAGNETIC GUIDANCE

In Figure 7, we compare the total travelled distance with respect to the number of data source nodes among these four schemes. We set link arc weight $a_l = t_l$ (i.e., the MNBOT travelled distance on link l). Note that Figure 6 gives the results of the MNBOT propagation delay on link l (say τ_l), since the MNBOT speed is 10^{-5} m/s, then $t_l = 10^{-5} \times \tau_l$ (in meters). With this link arc weight setting, the objective function of Problem (P) becomes to minimize the total MNBOT travelled distance. Figure 7 shows that LGA algorithm outperforms the other three heuristics, especially at large data source nodes. This is because, by setting the activation threshold $\Delta = |D|$, it sets higher activation threshold at large number of data source nodes. LGA algorithm that addresses

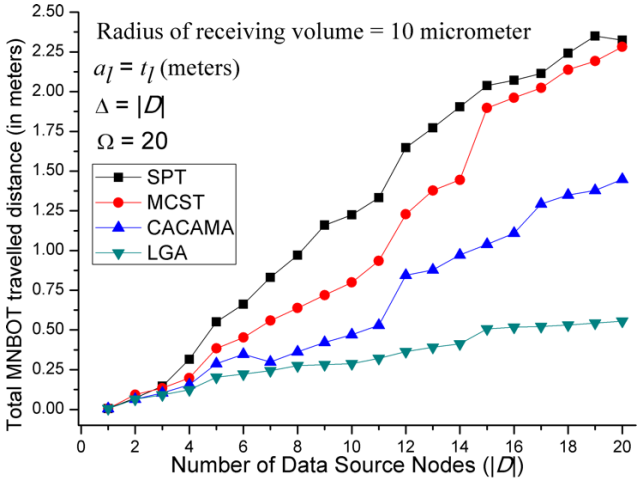

FIGURE 7. Total MNBOT travelled distance w.r.t. $|D|$.

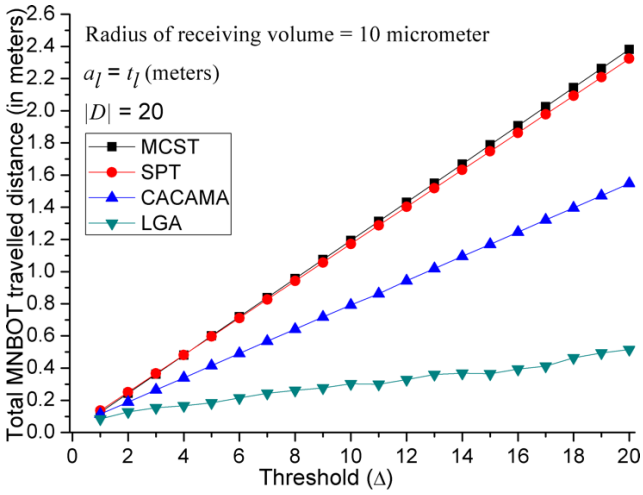

FIGURE 8. Total MNBOT travelled distance w.r.t. threshold (Δ).

the node activation constraint can reduce the total MNBOT travelled distance by the MNBOT aggregation strategy. And this saving is more significant at large number of data source nodes.

In the next experiment, we compare the solution quality of these four algorithms with respect to the activation threshold Δ. The number of data source nodes is fixed as 20 to examine the solution quality in various activation thresholds. Note that when setting the activation threshold to be 1, Problem (P) becomes traditional minimum cost routing problem. In this case, there is almost no difference between these four heuristics, which indicates that LGA algorithm is also a good solution approach in traditional minimum cost routing problem. Figure 8 also shows that LGA outperforms the other three heuristics especially at high activation threshold. Based on the results in Figure 7 and Figure 8, we conclude that LGA is more efficient than the other three heuristics especially at heavy network load (i.e., large number of data source nodes and high activation threshold).

Finally, we examine the activation time at the sink node. Recall that a node is activated only after all the relayed nodes

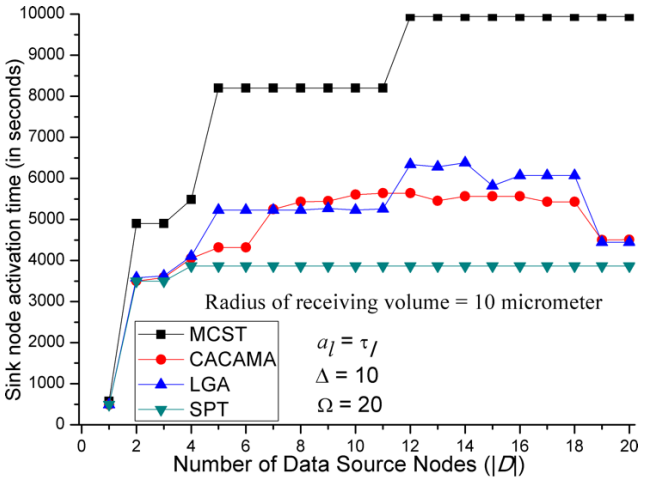

FIGURE 9. Sink node activation time w.r.t. $|D|$.

on the routing path back to the sink node have been activated. For instance, in Figure 2(a), the activation time of node S is the largest activated time among two paths (i.e., A→D→S and B→E→S). Note that the activation time at the sink node is not addressed in Problem (P). However, by setting a_l as the MNBOT propagation delay (i.e., τ_l) and the objective function to minimize the total MNBOT propagation delay, the LGA algorithm will implicitly identify the MNBOT routing decisions with reasonable activation time at the sink as shown in Figure 9.

In Figure 9, we see that SPT has the smallest activation time at the sink node because of its shortest path nature when link arc weight a_l is set as the MNBOT propagation delay on each link l. Even though LGA does not perform the best in this performance metric, the activation time at the sink is confined within acceptable range. In addition, it is very interesting to observe that the activation time at the sink node is decreased after $|D| \geq 18$. This shows that by leveraging on node activation constraint, minimizing the total propagation delay via the molecular aggregation strategy can help to stabilize the activation time at the sink node especially at high network load.

VI. CONCLUSION

Thanks to rapid progress of nanotechnologies, the advancement of MNBOTs show their huge potential in the cellular level biomedical applications. Instead of molecular diffusion-based communication, molecular communication and routing scheme based on guided MNBOTs is adopted in this paper with the advantages of faster propagation speed and better motion control. We first propose a generic EMAR model to capture the node activation property in existing biological processes (e.g., neuron signal propagation and cytokines communication in immune system). Then, an optimization-based algorithm (i.e., LGA) is devised to tackle this problem. The basic idea of LGA is to encourage molecular aggregation with considering the penalty cost from violating the node activation constraint. According to the computational

experiments, the LGA outperforms the other three heuristics (CACAMA, MCST and SPT) in terms of the total magnetic guiding cost. In addition, the MNBOT movement deviation along the trajectory of the magnetic field due to non-negligible interference from Brownian motion is also captured. Taking the MNBOT lifetime into account, diffusion based MNBOT routing scheme fails to reach the destination node with small receiving volume. Magnetic guidance in MNBOT routing can help to reduce the MNBOT travelling time, which is important in high precision bio-medical applications. With the consideration of the interplay between magnetic force and Brownian motion, LGA algorithm is still superior to the other three heuristics in terms of total travelled distance under different traffic loads and activation thresholds. By minimizing the total MNBOT propagation delay as the objective function, LGA algorithm can identify the routing decision in MNBOT networks with acceptable activation time at the sink node. Moreover, the activation time at the sink node decreases at high network load (i.e., $|D| \geq 18$). This shows that LGA algorithm is also applicable to the activation time aware applications, such as time sensitive immune response against bacteria and virus.

REFERENCES

[1] J. Li, B. Esteban-Fernández de Ávila, W. Gao, L. Zhang, and J. Wang, "Micro/nanorobots for biomedicine: Delivery, surgery, sensing, and detoxification," *Sci. Robot.*, vol. 2, no. 4, pp. 1–9, Mar. 2017.

[2] F. Mou, C. Chen, Q. Zhong, Y. Yin, H. Ma, and J. Guan, "Autonomous motion and temperature-controlled drug delivery of Mg/Pt-Poly(N-isopropylacrylamide) janus micromotors driven by simulated body fluid and blood plasma," *ACS Appl. Mater. Interfaces*, vol. 6, no. 12, pp. 9897–9903, 2014.

[3] G. Chatzipirpiridis, O. Ergeneman, J. Pokki, F. Ullrich, S. Fusco, J. A. Ortega, K. M. Sivaraman, B. J. Nelson, and S. Pané, "Electroforming of implantable tubular magnetic microrobots for wireless ophthalmologic applications," *Adv. Healthcare Mater.*, vol. 4, no. 2, pp. 209–214, 2015.

[4] E. Morales-Narváez, M. Guix, M. Medina-Sánchez, C. C. Mayorga-Martinez, and A. Merkoçi, "Micromotor enhanced microarray technology for protein detection," *Small*, vol. 10, pp. 2542–2548, Jul. 2014.

[5] Z. Wu, J. Li, B. Esteban-Fernández de Ávila, T. Li, W. Gao, Q. He, L. Zhang, and J. Wang, "Water-powered cell-mimicking Janus micromotor," *Adv. Funct. Mater.*, vol. 25, pp. 7497–7501, Dec. 2015.

[6] C. Chen, E. Karshalev, J. Li, F. Soto, R. Castillo, I. Campos, F. Mou, J. Guan, and J. Wang, "Transient micromotors that disappear when no longer needed," *ACS Nano*, vol. 10, no. 11, pp. 10389–10396, 2016.

[7] J. Li, I. Rozen, and J. Wang, "Rocket science at the nanoscale," *ACS Nano*, vol. 10, no. 6, pp. 5619–5634, 2016.

[8] B. Atakan, O. B. Akan, and S. Balasubramaniam, "Body area nanonetworks with molecular communications in nanomedicine," *IEEE Commun. Mag.*, vol. 50, no. 1, pp. 28–34, Jan. 2012.

[9] N. Farsad, H. B. Yilmaz, A. Eckford, C.-B. Chae, and W. Guo, "A comprehensive survey of recent advancements in molecular communication," *IEEE Commun. Surveys Tuts.*, vol. 18, no. 3, pp. 1887–1919, 3rd Quart., 2016.

[10] M. Pierobon and I. F. Akyildiz, "A physical end-to-end model for molecular communication in nanonetworks," *IEEE J. Sel. Areas Commun.*, vol. 28, no. 4, pp. 602–611, May 2010.

[11] T. Nakano and T. Suda, "Molecular communication using dynamic properties of oscillating and propagating patterns in concentration of information molecules," *IEEE Trans. Commun.*, vol. 65, no. 8, pp. 3386–3398, Aug. 2017.

[12] Y. Chen, P. Kosmas, P. S. Anwar, and L. Huang, "A touch-communication framework for drug delivery based on a transient microbot system," *IEEE Trans. Nanobiosci.*, vol. 14, no. 4, pp. 397–408, Jun. 2015.

[13] W. Gao, A. Uygun, and J. Wang, "Hydrogen-bubble-propelled zinc-based microrockets in strongly acidic media," *J. Amer. Chem. Soc.*, vol. 134, no. 2, pp. 897–900, 2012.

[14] J. G. S. Moo, S. Presolski, and M. Pumera, "Photochromic spatiotemporal control of bubble-propelled micromotors by a spiropyran molecular switch," *ACS Nano*, vol. 10, no. 3, pp. 3543–3552, 2016.

[15] T. Xu, F. Soto, W. Gao, V. Garcia-Gradilla, J. Li, X. Zhang, and J. Wang, "Ultrasound-modulated bubble propulsion of chemically powered microengines," *J. Amer. Chem. Soc.*, vol. 136, no. 24, pp. 8552–8555, 2014.

[16] J. E. Green, J. W. Choi, A. Boukai, Y. Bunimovich, E. Johnston-Halperin, E. DeIonno, Y. Luo, B. A. Sheriff, K. Xu, Y. S. Shin, H.-R. Tseng, J. F. Stoddart, and J. R. Heath, "A 160-kilobit molecular electronic memory patterned at 10^{11} bits per square centimetre," *Nature*, vol. 445, no. 7126, pp. 414–417, 2007.

[17] R. D. Astumian, "How molecular motors work—Insights from the molecular machinist's toolbox: The Nobel prize in chemistry 2016," *Chem. Sci.*, vol. 8, no. 2, pp. 840–845, Feb. 2017.

[18] P. L. Anelli, N. Spencer, and J. F. Stoddart, "A molecular shuttle," *J. Amer. Chem. Soc.*, vol. 113, no. 13, pp. 5131–5133, 1991.

[19] R. A. Bissell, E. Córdova, A. E. Kaifer, and J. F. Stoddart, "A chemically and electrochemically switchable molecular shuttle," *Nature*, vol. 369, no. 6476, pp. 133–137, 1994.

[20] A. I. Basbaum, D. M. Bautista, G. Scherrer, and D. Julius, "Cellular and molecular mechanisms of pain," *Cell*, vol. 139, no. 2, pp. 267–284, 2009.

[21] B. E. Cairns, P. Svensson, K. Wang, S. Hupfeld, T. Graven-Nielsen, B. J. Sessle, C. B. Berde, and L. Arendt-Nielsen, "Activation of peripheral NMDA receptors contributes to human pain and rat afferent discharges evoked by injection of glutamate into the masseter muscle," *J. Neuro Physiol.*, vol. 90, no. 4, pp. 2098–2105, 2003.

[22] N. I. Markevich, M. A. Tsyganov, J. B. Hoek, and B. N. Kholodenko, "Long-range signaling by phosphoprotein waves arising from bistability in protein kinase cascades," *Mol. Syst. Biol.*, vol. 2, no. 1, p. 61, 2006.

[23] S. Demotz, H. M. Grey, and A. Sette, "The minimal number of class II MHC-antigen complexes needed for T cell activation," *Science*, vol. 249, no. 4972, pp. 1028–1030, 1990.

[24] A. Grakoui, S. K. Bromley, C. Sumen, M. M. Davis, A. S. Shaw, P. M. Allen, and M. L. Dustin, "The immunological synapse: A molecular machine controlling T cell activation," *Science*, vol. 285, no. 5425, pp. 221–227, 1999.

[25] E. Narni-Mancinelli, S. Ugolini, and E. Vivier, "Tuning the threshold of natural killer cell responses," *Current Opinion Immunol.*, vol. 25, no. 1, pp. 53–58, 2013.

[26] H.-H. Yen, X. Wang, and D. Wang, "QoS aware molecular activation and communication scheme in molecular nanoscale sensor networks," in *Proc. IEEE Int. Conf. e-Health Netw., Appl. Services (Healthcom)*, Sep. 2016, pp. 1–6.

[27] R. K. Ahuja, T. L. Magnanti, and J. B. Orlin, *Network Flows: Theory, Algorithms, and Applications*. Upper Saddle River, NJ, USA: Prentice-Hall, 1993.

[28] X. Ma, X. Wang, K. Hahn, and S. Sánchez, "Motion control of urea-powered biocompatible hollow microcapsules," *ACS Nano*, vol. 10, no. 3, pp. 3597–3605, 2016.

[29] P. Mörters and Y. Peres, *Brownian Motion*. Cambridge, U.K.: Cambridge Univ. Press, 2010.

[30] R. L. E. Cano, H. Damaris, and E. Lopera, "Introduction to T and B lymphocytes," in *Autoimmunity: From Bench to Bedside*, J.-M. Anaya, R. A. Levy, A. Rojas-Villarraga, and Y. Shoenfeld, Eds. Bogota, Colombia: El Rosario Univ. Press, 2013, ch. 5. [Online]. Available: https://www.ncbi.nlm.nih.gov/books/NBK459471/

[31] D. Cappelleri, D. Efthymiou, A. Goswami, N. Vitoroulis, and M. Zavlanos, "Towards mobile microrobot swarms for additive micromanufacturing," *Int. J. Adv. Robot. Syst.*, vol. 11, no. 9, p. 150, 2014.

[32] A. Tsioliaridou, C. Liaskos, E. Dedu, and S. Ioannidis, "Packet routing in 3D nanonetworks: A lightweight, linear-path scheme," *Nano Commun. Netw.*, vol. 12, pp. 63–71, Jun. 2017.

[33] K. Jensen, J. Weldon, H. Garcia, and A. Zettl, "Nanotube radio," *Nano Lett.*, vol. 7, no. 11, pp. 3508–3511, 2007.

[34] J. M. Jornet and I. F. Akyildiz, "Femtosecond-long pulse-based modulation for terahertz band communication in nanonetworks," *IEEE Trans. Commun.*, vol. 62, no. 5, pp. 1742–1754, May 2014.

[35] J. Yan, M. Zhou, and Z. Ding, "Recent advances in energy-efficient routing protocols for wireless sensor networks: A review," *IEEE Access*, vol. 4, pp. 5673–5686, Aug. 2016.

[36] R. Mitra and S. Sharma, "Proactive data routing using controlled mobility of a mobile sink in wireless sensor networks," *Comput. Elect. Eng.*, vol. 70, pp. 21–36, Aug. 2018.
[37] M. Huang, W. Liu, T. Wang, H. Song, X. Li, and A. Liu, "A queuing delay utilization scheme for on-path service aggregation in services oriented computing networks," *IEEE Access*, vol. 7, pp. 23816–23833, 2019.
[38] J. Li, W. Liu, T. Wang, H. Song, X. Li, F. Liu, and A. Liu, "Battery-friendly relay selection scheme for prolonging the lifetimes of sensor nodes in the Internet of Things," *IEEE Access*, vol. 7, no. 1, pp. 33180–33201, 2019.

HONG-HSU YEN (M'06) received the B.S. degree in industrial engineering from National Tsing Hua University, in 1990, and the M.S. degree in electrical engineering and the Ph.D. degree in information management from National Taiwan University, in 1995 and 2001, respectively. He joined the Faculty of the Department of Information Management, Shih Hsin University, in 2001, where he is currently a Professor. His research interests include biomedical engineering, healthcare technologies, wireless sensor networks, and optimization. He is the author of one book and more than 50 articles. He holds two patents. He serves as an Editor for ISRN Sensor Networks and the Lead Guest Editor for the *International Journal of Distributed Sensor Networks: Special Issue on Recent Advances in Wireless Visual Sensor Networks*, in 2013. He was a recipient of the Outstanding Research Award from Shih Hsin University, in 2006, 2011, and 2015.

XINHENG WANG (M'04–SM'14) received the B.E. and M.Sc. degrees in electrical engineering from Xi'an Jiaotong University, Xi'an, China, in 1991 and 1994, respectively, and the Ph.D. degree in electronics and computer engineering from Brunel University London, Uxbridge, U.K., in 2001.

He was with Higher Education Institutions in England, Wales, and Scotland on various academic roles. He has been an Investigator or a Co-Investigator of more than 20 research projects sponsored from EU, U.K. EPSRC, Innovate U.K., China NSFC, and industry. He is currently a Professor with the Department of Electrical and Electronic Engineering, Xi'an Jiaotong-Liverpool University, Suzhou, China. He has authored or coauthored more than 150 referred articles. He holds 15 granted patents, including one U.S., one Japan, four South Korea, and nine China patents. His current research interests include wireless networks, indoor positioning, the Internet of Things (IoT), and big data analytics for smart airport services, where he has developed the world's first smart trolley with Chigoo Interactive. His research has led to a few commercial products in condition monitoring, wireless mesh networks, and acoustic localization and user-centric routing and navigation.

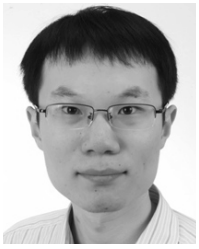

DONG WANG (S'17) received the B.Sc. degree in electronic information science and technology from Qufu Normal University, China, in 2012, and the M.Sc. degree in telecommunication systems from Swansea University, U.K., in 2014. He is currently pursuing the Ph.D. degree in computing with the University of the West of Scotland, U.K. His research interests include modeling and optimization of complex heterogeneous networks, which have been developed in beyond 5G airborne networks, the Internet of Things, and wireless ad hoc networks.

HORNG-TWU LIAW received the B.S. degree in computer engineering from National Chiao Tung University, in 1986, the M.S. degree in applied mathematics from National Chung Hsing University, in 1989, and the Ph.D. degree in electronic engineering from National Taiwan University, in 1992. He joined the Faculty of the Department of Information Management, Shih Hsin University, in 1993, where he is currently a Professor and the Vice President. His research interests include information security, algorithms, and e-commerce technologies.